Applied Catalysis B: Environmental 268 (2020) 118752

Contents lists available at ScienceDirect

Applied Catalysis B: Environmental

journal homepage: www.elsevier.com/locate/apcatb

Mechanistic study of non-thermal plasma assisted CO_2 hydrogenation over Ru supported on MgAl layered double hydroxide

Shanshan Xu[a], Sarayute Chansai[a], Yan Shao[b], Shaojun Xu[a], Yi-chi Wang[c], Sarah Haigh[c], Yibing Mu[a], Yilai Jiao[d], Cristina E. Stere[a], Huanhao Chen[a,*], Xiaolei Fan[a,*], Christopher Hardacre[a,*]

[a] Department of Chemical Engineering and Analytical Science, The University of Manchester, Oxford Road, Manchester M13 9PL, United Kingdom
[b] School of Biotechnology and Health Sciences, Wuyi University, Jiangmen 52920, China
[c] Department of Materials, The University of Manchester, Oxford Road, Manchester M13 9PL, United Kingdom
[d] Shenyang National Laboratory for Materials Science, Institute of Metal Research, Chinese Academy of Sciences, 72 Wenhua Road, Shenyang 110016, China

ARTICLE INFO

Keywords:
Non-thermal plasma (NTP)
Ru/MgAl layered double hydroxide (LDH)
CO_2 hydrogenation
DRIFTS

ABSTRACT

Carbon dioxide (CO_2) hydrogenation to value-added molecules is an attractive way to reduce CO_2 emission *via* upgrading. Herein, non-thermal plasma (NTP) activated CO_2 hydrogenation over Ru/MgAl layered double hydroxide (LDH) catalysts was performed. The catalysis under the NTP conditions enabled significantly higher CO_2 conversions (~85 %) and CH_4 yield (~84 %) at relatively low temperatures compared with the conventional thermally activated catalysis. Regarding the catalyst preparation, it was found that the reduction temperature can affect the chemical state of the metal and metal-support interaction significantly, and thus altering the activity of the catalysts in NTP-driven catalytic CO_2 hydrogenation. A kinetic study revealed that the NTP-catalysis has a lower activation energy (at ~21 kJ mol^{-1}) than that of the thermal catalysis (*ca.* 82 kJ mol^{-1}), due to the alternative pathways enabled by NTP, which was confirmed by the comparative *in situ* diffuse reflectance infrared Fourier (DRIFTS) coupled with mass spectrometry (MS) characterisation of the catalytic systems.

1. Introduction

Catalytic hydrogenation of carbon dioxide (CO_2) is an appealing way to produce fuels and chemical building blocks such as methane (CH_4) and methanol. The hydrogenation of CO_2 at atmospheric pressure yields mainly CH_4 (*i.e.* CO_2 methanation), and/or CO (*via* the reverse water-gas shift reaction) [1]. CO_2 methanation is considered important in the "power-to-gas" process, enabling the large-scale chemical storage of hydrogen (H_2) generated by sustainable pathways (*e.g.* using solar energy and hydropower) [2]. Additionally, the synthetic (or substitute) natural gas from the reaction can be easily stored and transported, or directly injected into the existing industrial natural gas infrastructures [3]. The reaction (Eq. 1) is highly exothermic and kinetically limited accordingly, catalytic CO_2 methanation with high conversions at low temperatures is challenging. Therefore, to promote direct CO_2 activation, the development of highly active and stable catalysts at mild thermal conditions (*e.g.* $T < 250$ °C) [4], as well as new processes for activating the catalysis, is still urgently needed.

$$CO_2 + 4H_2 \rightarrow CH_4 + 2H_2O \; \Delta_r H^0_{298K} = -164.94 \text{kJ mol}^{-1} \quad (1)$$

Extensive studies have been performed to develop metal catalysts for CO_2 methanation, among which Ni, Ru and Rh have been revealed as effective candidates [5]. Although nickel-based catalysts are relatively cost-effective and earth abundant, they are prone to deactivation due to carbon deposition, sintering and chemical poisoning [6]. Conversely, Ru-based catalysts are relatively stable, as well as being highly active for CO_2 methanation. Layered double hydroxides (LDHs) have the general formula of $[M^{2+}_{1-x} M^{3+}_{x} (OH)]^{z+} A^{n-}_{z/n} \cdot mH_2O$, in which M^{2+} and M^{3+} occupy the octahedral holes in a brucite-like layer and A^{n-} represents the exchangeable interlayer anions to compensate the positive charge on the layers, being widely employed as catalysts, catalyst precursors and catalyst supports [7]. As the catalyst support, LDH offers: (*i*) 6-fold coordinated OH− groups with divalent and trivalent cations, which can facilitate chemisorption and activation of CO_2, (*ii*) turntable electronic structure (or basicity) of the surface of LDHs as well as the layered double oxide (LDOs) produced by calcination of LDH, and (*iii*) coordinatively unsaturated active sites (*e.g.* low-

* Corresponding authors.
E-mail addresses: c.hardacre@manchester.ac.uk (H. Chen), xiaolei.fan@manchester.ac.uk (X. Fan), huanhao.chen@manchester.ac.uk (C. Hardacre).

https://doi.org/10.1016/j.apcatb.2020.118752
Received 22 November 2019; Received in revised form 14 January 2020; Accepted 10 February 2020
Available online 11 February 2020

coordinated steps, edges and corner atoms) to promote the metal dispersion [8,9]. To date, Ni−Al catalysts derived from Ni_3Al LDH has shown high CO_2 conversions (*e.g.* 86 %) at 300 °C due to the high metal surface area (*e.g.* ~52 m_{Ni}^2 g_{cat}^{-1}) and dispersions (*e.g.* 16 %) [10].

Non-thermal plasma (NTP) dissociates and activates gaseous species to produce a variety of active electrons, ions and radicals, being able to participate in surface reactions over a catalyst under relatively mild conditions (*i.e.* atmospheric pressure and low bulk temperatures < ~200 °C) compared to the conventional thermally activated catalysis [11,12]. Previously, NTP-catalysis was highly effective for promoting kinetically and/or thermodynamically limited reactions, such as CO_2 dry reforming [13] and water gas shift reactions [14,15], without an external heat source. Recently, NTP-assisted catalytic CO_2 hydrogenation over Ni/Al_2O_3 catalysts has been demonstrated, in which the conversion of CO_2 was improved significantly (by 60 % compared to the NTP-promoted gas-phase reactions) at ~150 °C [16]. Therefore, NTP-catalysis represents an alternative to thermal catalysis due to the presence of the plasma-generated reactive species and plasma-catalyst interactions [17]. However, the specific activation mechanism in NTP-catalysis depends on various factors including the type of catalyst and reaction, and *in situ* characterisation of the NTP-catalysis (such as diffuse reflectance infrared Fourier transform, DRIFTS, and extended X-ray absorption fine structure, EXAFS) was proven to be beneficial to develop insights into the complex system [15,18,19].

Herein, a series of Ru catalysts with different Ru loading (0.4 %, 1.0 %, 2.5 % and 5%) supported on MgAl LDHs were developed and reduced at different temperatures (160–600 °C). The developed Ru catalysts were used in the comparative and systematic catalytic tests for CO_2 hydrogenation under both NTP and thermal (at 250 °C or 300 °C) conditions, aiming at developing an understanding of the catalysis under the NTP conditions used. NTP-catalysis systems were also investigated *in situ* using a combined DRIFTS-mass spectrometry (MS), in which the dynamics of surface species during the NTP-activated CO_2 hydrogenation provide useful information to allow the development of reaction mechanism of the system under study.

2. Experimental

2.1. Chemicals

Ruthenium(III) chloride trihydrate (**$RuCl_3{\cdot}3H_2O$**), magnesium nitrate hexahydrate ($Mg(NO_3)_2{\cdot}6H_2O$, > 99 %), aluminum nitrate nonahydrate ($Al(NO_3)_3{\cdot}9H_2O$, > 98 %) and urea (BioUltra, > 99.5 %) were purchased from Sigma Aldrich and used without further purification.

2.2. Characterisation of catalysts

The catalysts were characterised by scanning electron microscopy (SEM), high-resolution transmission electron microscopy (HRTEM), X-ray diffraction (XRD), X-ray photoelectron spectroscopy (XPS), inductively coupled plasma optical emission spectroscopy (ICP-OES), CO chemisorption, nitrogen (N_2) physisorption analysis, hydrogen temperature programmed reduction (H_2-TPR) and CO_2 temperature programmed desorption (CO_2-TPD). The relevant technical details of the characterisation techniques are presented in the Supporting Information (SI).

2.3. Synthesis of MgAl layered double hydroxides (LDHs)

MgAl LDH was synthesised using a urea-assisted coprecipitation method. Typically, $Mg(NO_3)_2{\cdot}6H_2O$ (0.01 mol), $Al(NO_3)_3{\cdot}9H_2O$ (0.005 mol) and urea (0.005 mol) were first dissolved in 50 mL deionised water and stirred for 30 min. The resulting homogeneous solution was then transferred into a Teflon-lined stainless-steel autoclave, sealed and hydrothermally treated at 110 °C for 24 h. After cooling the system down to room temperature (RT), the solid product was separated by centrifugation, washed repeatedly with deionised water, and finally dried at 70 °C overnight.

2.4. Preparation of Ru/MgAl catalysts

Ru/MgAl catalysts were prepared using the conventional wet impregnation method. Firstly, the obtained MgAl LDH (1.5 g) was suspended in water (30 mL), then 0.07 g $RuCl_3{\cdot}3H_2O$ was added in the suspension. After vigorous stirring for 3 h, the precipitate was filtered, washed with deionised water and dried at 60 °C for 12 h. Different theoretical loadings of Ru (0.4 %, 1.0 %, 2.5 % and 5%) on MgAl LDH were achieved by adjusting the concentration of $RuCl_3{\cdot}3H_2O$ during impregnation. The obtained dry solids were subsequently reduced under a H_2 atmosphere at different reduction temperatures ranging from 160 to 600 °C for 2 h, with a heating rate of 5 °C min^{-1}. After reduction, the samples were cooled to RT naturally. Based on the theoretical metal loading and the reduction temperature, the catalysts developed have been denoted as *x*% Ru/MgAl-R*y* (where *x* refers to the theoretical Ru loading and *y* is the reduction temperature). The actual metal loading was determined by ICP-OES (SI).

2.5. NTP-activated catalytic CO_2 hydrogenation

The catalytic activity, selectivity and stability of the prepared catalysts were assessed at atmospheric pressure in a dielectric barrier discharge (DBD, 6 mm O.D. × 4 mm I.D.) flow reactor (Fig. S1). An aluminium foil wrapped around outside of the quartz tube was used as the high voltage electrode, while a stainless-steel rod (1 mm O.D.) placed in the centre of the quartz tube was used as the ground electrode. The discharge length and gap of the DBD reactor were 10 mm and 1.5 mm, respectively. The electrical parameters of NTP were monitored using an oscilloscope (Tektronix TBS1072B) which was connected to the reactor through a high voltage probe (Tektronix, P6015). Typically, 100 mg catalysts (pelletised with particle size of 250–425 μm) were loaded in the discharge zone between two quartz wool plugs. As the catalysts can be re-oxidised due to exposition to air at RT, the catalyst was treated *in situ* before NTP-catalysis (at 6.5 kV) using pure H_2 as the discharge gas (50 mL min^{-1} for 20 min.). For the reaction, the gas mixture of H_2 and CO_2 (molar ratio of 4:1) was fed into the DBD plasma reactor. The total flow rate and space velocity of the gas mixture were 50 mL min^{-1} and 30,000 mL (STP) g_{cat}^{-1} h^{-1}, respectively. The applied voltage was from 5.5 kV to 7.5 kV, while a constant frequency of 20.5 kHz was used. The outlet gas composition was analysed by a two-channel on-line gas chromatography GC equipped with an Elite-Carbon molecular sieve packed column N 9303926, a thermal conductivity detector (TCD) and a flame ionisation detector (FID). For each measurement, three samples of gas products were taken and analysed under steady-state conditions. The produced water was condensed by a glass water trap cooled by an ice bath and the total flowrate of the gas products was measured by a bubble-flow meter for the calculation of CO_2 conversion and CH_4 selectivity (as defined in the SI). Control experiments, *i.e.* catalyst-free CO_2 hydrogenation under NTP (gas phase reactions) and NTP-assisted CO_2 hydrogenation over LDHs were performed under the same conditions.

For comparison, thermally activated catalysis at 250 °C and 300 °C was carried out at atmospheric pressure as well. Typically, the Ru/MgAl catalysts were first treated *in situ* at 250 °C for 1 h under a 20 % H_2/Ar flow at 100 mL min^{-1}. Then the gas mixture of CO_2 and H_2 (volume ratio = 1:4) was fed into the reactor at 50 mL min^{-1}. The temperature of the catalyst bed was monitored by placing a K-type thermocouple in the middle of the catalyst bed. CO_2 (X_{CO2}) conversion, selectivity towards CH_4 (S_{CH4}) and CO (S_{CO}), CH_4 yield, Carbon balance and turnover frequency (TOF) were determined accordingly to evaluate the catalytic performance (SI).

2.6. In situ DRIFTS-MS characterisation of NTP-activated CO_2 hydrogenation

The experimental setup for the NTP-DRIFTS was described in detail elsewhere [15] (Fig. S2). The catalyst was loaded into the IR cell and pre-treated in a 10 % H_2/Ar flow under the plasma (applied voltage: 5.0 kV, frequency: 23.5 kHz) for 30 min. Then the gas reactant (1 vol.% CO_2 and 4 vol. % H_2 with Ar balance) was introduced into the cell to initiate the reaction. The use of Ar balance in DRIFTS was to avoid the signal saturation of IR spectra and MS signal. A constant peak voltage of 5.0 kV and pulse frequency of 23.5 kHz were employed to avoid arcing between the electrodes. IR spectra were recorded every 60 s with a resolution of 4 cm^{-1} and analysed by the OPUS software.

3. Result and discussion

3.1. NTP-activated CO_2 hydrogenation

The performance of the 2.5 % Ru/MgAl catalysts in NTP-activated CO_2 hydrogenation was studied in reference to the control experiments (*i.e.* empty tube for gas phase reaction and with the MgAl LDH support packing under the NTP conditions). Fig. 1a and b shows insignificant CO_2 conversion and selectivity to CH_4 as a function of plasma voltage/power in the two control experiments. For the blank reactor, only 5% conversion of CO_2 was achieved due to the NTP-assisted dissociation of CO_2 to CO in the gas phase. Similarly, the NTP system with the MgAl LDH packing was only selective to CO with a CO_2 conversion of ~10 % (due to the CO_2 adsorption on MgAl LDH which facilitates the NPT dissociation [20], the CO selectivity and carbon balance are shown in Fig. S3). Conversely, the NTP-catalysis system using the packing of 2.5 % Ru/MgAl catalysts showed significant CO_2 conversions and selectivity to CH_4 of > 68 % and > 95 %, respectively, at voltages above 6.5 kV, demonstrating the promoting effect of NTP on the catalysis.

For all 2.5 % Ru/MgAl catalysts, the activity profile under NTP conditions (*e.g.* the calculated specific reaction rates, TOF, in Fig. 1d) shows a similar trend as a function of the discharge voltage/power. Specifically, the CO_2 conversion (Fig. 1a) and CH_4 selectivity/yield (Fig. 1b and c) show an initial steep increase with an increase of the voltage which then decrease slightly on increasing the voltage to 7.5 kV. The initial increase of CO_2 conversion and CH_4 selectivity

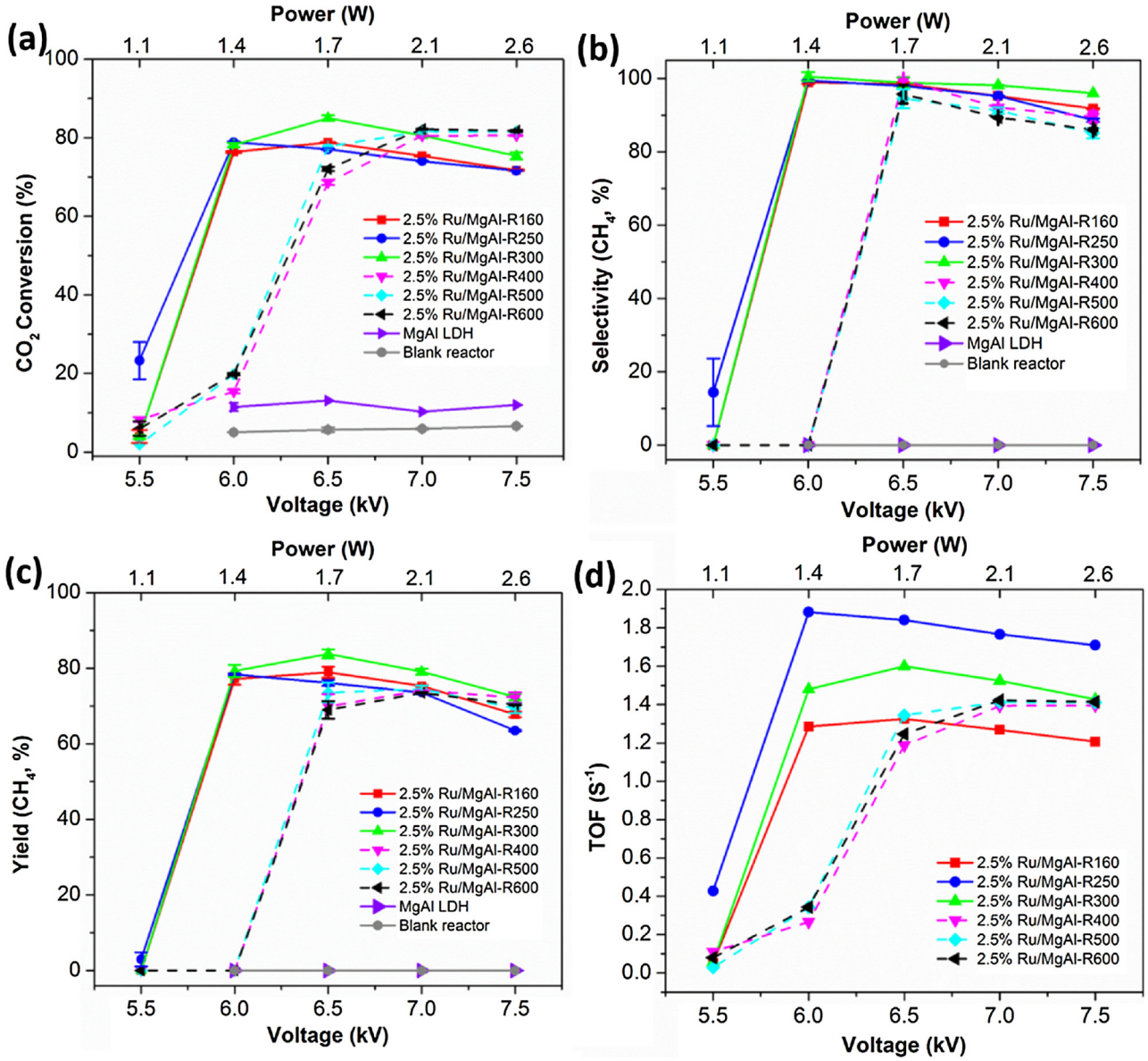

Fig. 1. Performance of NTP-activated catalytic CO_2 hydrogenation as a function of voltage/power over the 2.5 % Ru/MgAl catalysts reduced at different temperatures in reference to the control experiments. (a) CO_2 conversion, (b) CH_4 selectivity, (c) CH_4 yield and (d) TOF.

corresponds to the increased input energy under NTP conditions, *i.e.* the catalysis requires the energy input over the threshold value at ~5.5 kV to be activated under the NTP conditions. The gradual decrease in the selectivity to CH_4 may be related to the methane steam reforming reactions under NTP, producing CO and other hydrocarbons [21] (which were detected by GC as shown in Fig. S4, *i.e.* the peak for C_2H_x in the outlet gas mixture at 7.5 kV). Interestingly, the reduction temperature used for treating the 2.5 % Ru/MgAl catalysts had a considerable effect on their catalytic performance under NTP conditions. The 2.5 % Ru/MgAl catalysts reduced at < 300 °C showed a higher initial activity compared with the catalysts reduced at > 300 °C. For example, at 6.0 kV, the 2.5 % Ru/MgAl-R300 catalyst showed about 80 % CO_2 conversion with 99.5 % selectivity to CH_4 and 79 % CH_4 yield, while the catalysts reduced at > 300 °C only gave < 20 % conversion and zero CH_4 formation. Based on the comparison of TOF values at 6.0 kV, 2.5 % Ru/MgAl-R250 gives a TOF value of 1.9 s^{-1}, representing a > 7-fold increase compared with the TOF value of 2.5 % Ru/MgAl-R400. To explain the effect of reduction temperature on the catalytic activity of the 2.5 % Ru/MgAl catalysts, the catalysts were characterised and these results correlated with the reaction data.

Considering that the 2.5 % Ru/MgAl-R300 catalyst displayed relatively high CO_2 conversion and CH_4 yield, catalysts with different Ru loading were prepared and reduced at 300 °C, and then used in the comparative evaluations under both NTP and thermal conditions (Figs. 2 and S5). The highest CO_2 conversion was obtained with an optimal 2.5 % Ru loading. By increasing the Ru loading further to 5%, the catalytic activity decreased. This result could be attributed to the aggregation of Ru NPs on the support surface when excessive Ru was loaded, which led to the reduced activity (Fig. S6). In general, regardless the variation of Ru loading on the catalysts, the NTP activation significantly enhanced the CO_2 conversion compared with the thermal activation (Fig. 2a and b). In detail, NTP activation enabled high CO_2 conversions (~85 %) at 6.5 kV and relatively low average temperature of ~129 °C (by Infrared (IR) thermometer). Conversely, under the thermal condition at 250 °C, only 13.7 % and 3.7 % CO_2 conversion were achieved, respectively, over 2.5 % and 5% Ru/MgAl-R300 catalysts, while no CO_2 conversion was found for the catalysts with low Ru loadings (*i.e.* 0.4 % and 1.2 % Ru/MgAl-R300 catalysts, which enabled 1.5 % and 8.1 % CO_2 conversion, respectively, at 300 °C, as shown in Fig. 2a). Accordingly, to develop a mechanistic understanding of the NTP catalysis, relevant kinetic studies were performed (details of the kinetic calculations are presented in the SI). Fig. 2c shows that the thermal system exhibits the typical Arrhenius behaviour with the calculated activation energy over the 2.5 % Ru/MgAl-R160, R300 and R600 catalysts being 68, 82 and 113 kJ mol^{-1}, respectively, while the energy barriers of the NTP-catalysis were 30, 21 and 43 kJ mol^{-1}, respectively, which is about 3 times smaller than that required by the thermal activation [22] (Table 1). The findings from the kinetic study suggest that plasma-catalyst interactions may enable alternative pathways for promoting CO_2 hydrogenation.

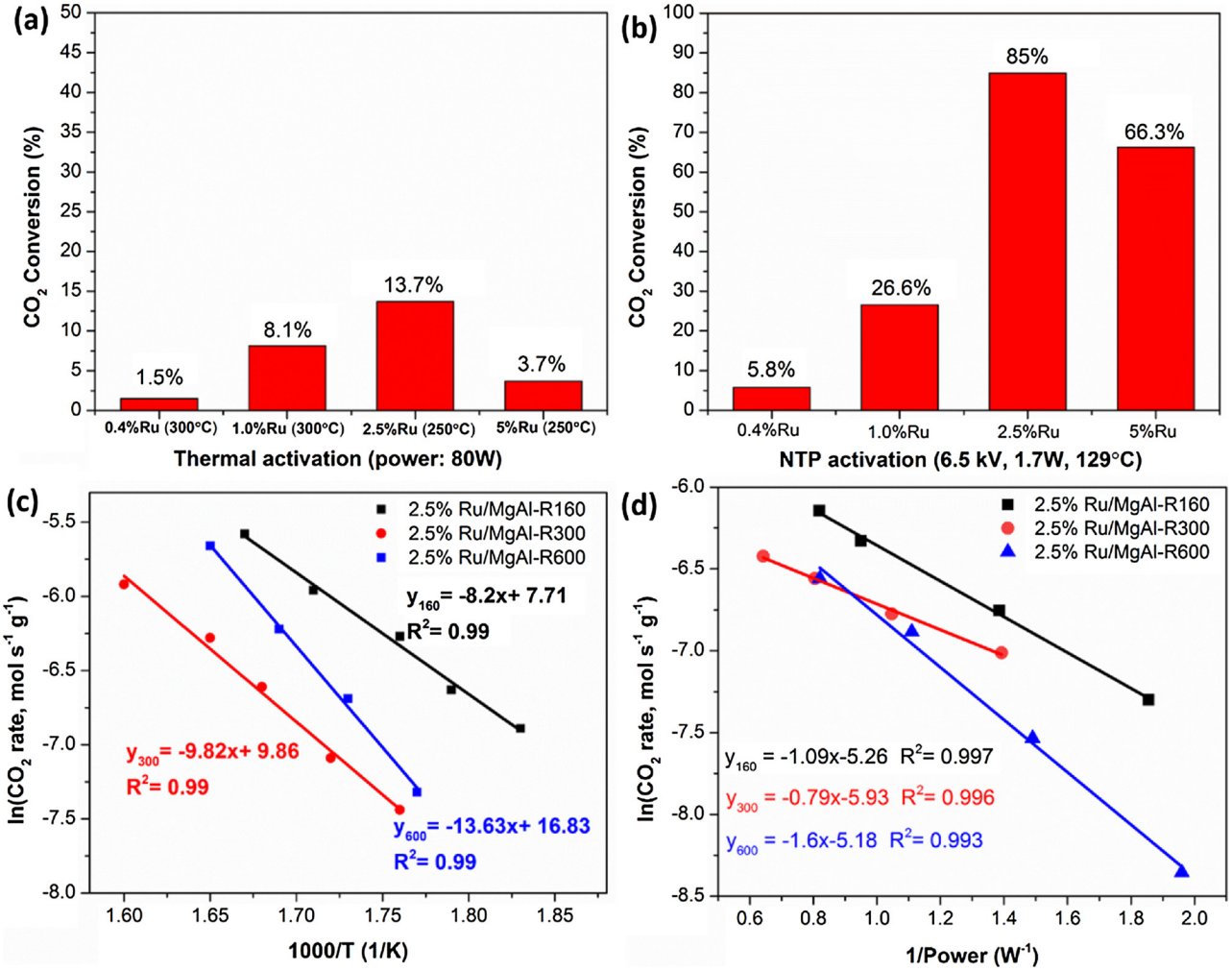

Fig. 2. Comparison of the performance of catalytic CO_2 hydrogenation over the 0.4 %, 1.0 %, 2.5 % and 5% Ru/MgAl catalysts reduced at 300 °C under (a) thermal conditions at 250 or 300 °C; (b) NTP condition at 6.5 kV (20.5 kHz, 1.7 W). Determination of the activation energy over the 2.5 % Ru/MgAl catalysts reduced at 160 °C, 300 °C and 600 °C (c) under thermal and (d) NTP conditions.

Table 1
Activation energy calculated for catalytic CO_2 hydrogenation over 2.5 % Ru/MgAl catalysts (reduced at 160 °C, 300 °C and 600 °C, respectively) by thermal and plasma activation.

Catalysts	E_a (kJ mol^{-1}) Thermal activation	E_a (kJ mol^{-1}) NTP activation
2.5 % Ru/MgAl-R160	68	30
2.5 % Ru/MgAl-R300	82	21
2.5 % Ru/MgAl-R600	113	43

The NTP-catalysis system (at 6.5 kV, 20.5 kHz) also showed good stability, which was demonstrated by the 2.5 % Ru/MgAl-R300 catalyst in the longevity test (Fig. 3a). Under the NTP condition, the catalyst displayed high activity (about 84 % CO_2 conversion) and no deactivation over 600 min time on stream and maintained a high selectivity to CH_4 of ~98.4 %. The stability of the NTP-catalysis system may be due to the absence of metal sintering, which is common in the conventional thermal catalysis, especially at high temperatures. The post-reaction TEM characterisation of the catalyst (as shown in Fig. 3b and c) provides the information on particle size of Ru NPs after the longevity test showing 1.9 ± 0.4 nm which is comparable to that of the fresh catalyst.

3.2. Effect of reduction temperature on the property of the catalysts

To understand the effect of the reduction temperature on the catalytic activity of the resulting catalysts, XRD analysis was performed to characterise the as-reduced catalysts (Figs. 4 and S7). The characteristic diffraction peaks of MgAl LDH support at 2θ = 12°, 23.9°, 35° and 39.8° are ascribed to the (003), (006), (012) and (015) reflections, corresponding to a well-defined hydrotalcite structure. Accordingly, the basal spacing value (d_{003}) of MgAl-LDH support is calculated as 0.80 nm, being similar to that of the LDH with CO_3^{2-} anions in the layer [23]. All the as-prepared 2.5 % Ru/MgAl catalysts did not show the relevant diffraction peaks associated with the crystalline Ru phases, indicating that Ru is finely dispersed on the support which is consistent with the TEM results. After the reduction of $RuCl_3$-impregnated MgAl LDH at 160 °C, XRD analysis of the resulting catalyst (*i.e.* 2.5 % Ru/MgAl-R160) showed the relatively reduced peak intensities and the shift of peak positions. However, the XRD patterns of 2.5 % Ru/MgAl-R160 catalyst is still comparable to that of the MgAl LDH support. Conversely, by increasing the reduction temperature from 160 °C to 300 °C, the characteristic diffraction peaks of MgAl support in the resulting catalysts disappeared, leaving two broad diffraction peaks by (003) and (110) facets with comparatively low intensities, which suggests dehydration of the support at high temperatures and a reduced crystallinity of the hydrotalcite structure. By increasing the reduction temperature

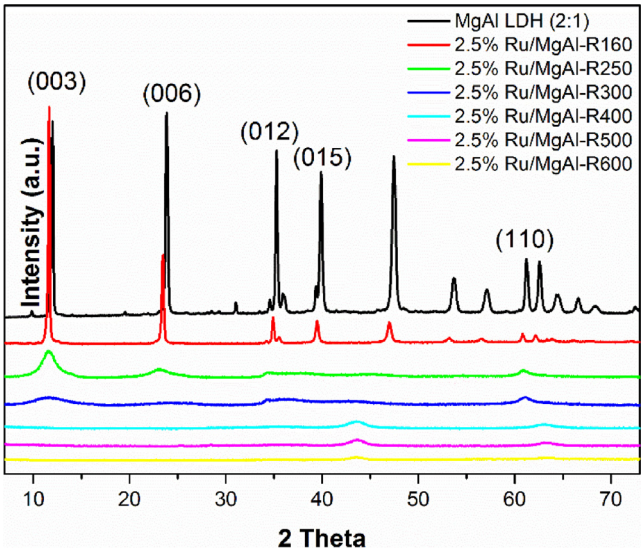

Fig. 4. XRD patterns of MgAl LDH and fresh 2.5 % Ru/MgAl catalysts reduced at different temperatures of 160 °C, 250 °C, 300 °C, 400 °C, 500 °C and 600 °C, respectively, under H_2.

from 300 °C to 600 °C, diffraction peaks associated with the LDH phase disappeared completely, suggesting the phase transition from LDH to $Mg_2(Al)O$ layer double oxide (LDO) [24]. Additionally, two diffraction peaks at 43.6° and 63.4° (with the low intensity) were detected, corresponding to crystalline MgO phase, confirming the formation of the $Mg_2(Al)O$ mixed oxide phase with the incorporation of Al^{3+} into the MgO lattice [25].

SEM and HRTEM were performed (Figs. 5 and S8) to understand the effect of reduction temperature on Ru particle size and dispersion in the catalysts. According to the SEM micrographs (Fig. S8), the MgAl LDH nanocrystals under study (by hydrothermal synthesis) exhibits the well-defined hexagonal shape with average crystal sizes of ~2.7 μm, being consistent with the XRD results. After the reduction treatments at different temperatures, the shape of LDH remained intact. The elemental mapping analysis of the materials (Figs. S9 − S11) shows that the Ru is uniformly distributed on the support. HRTEM analysis revealed the particle size distribution of the resulting catalysts (Fig. 5). The catalysts reduced at < 300 °C showed an average particle size of Ru of 1.6 − 1.7 nm, while it is 1.9 − 2.0 nm for the catalysts reduced at above 400 °C (Table S4). The slight increase of the Ru NPs size could be attributed to the phase transformation of the support (*i.e.* from LDH to LDO). Previous study showed that the hydrogenation activity is positively correlated with the Ru particle size, and relatively large Ru NPs (< 3 nm)

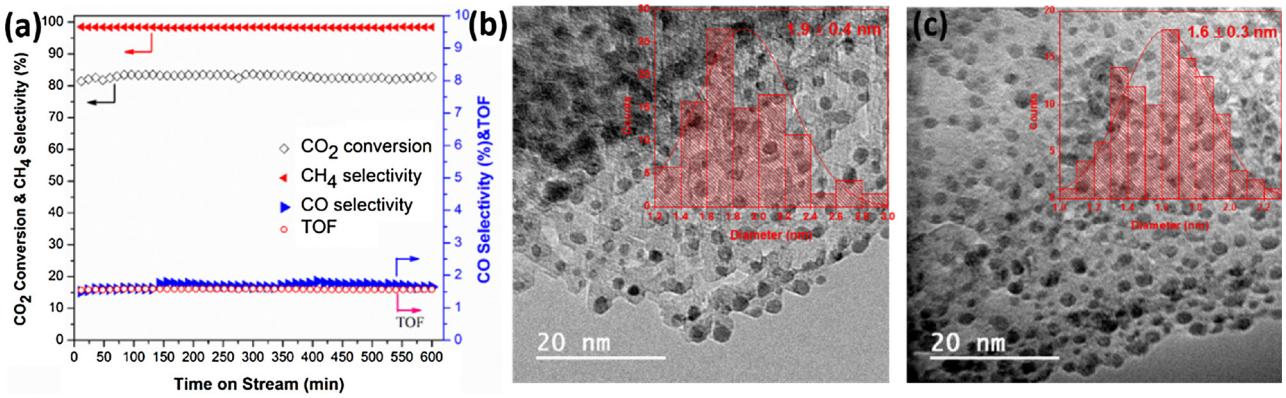

Fig. 3. (a) Stability test of the 2.5 % Ru/MgAl-R300 catalyst for catalytic CO_2 hydrogenation under the NTP condition (H_2/CO_2 = 4, WHSV = 30,000 mL STP g_{cat}^{-1} h^{-1}); (b) TEM image and particle size distribution of the used 2.5 % Ru/MgAl-R300 catalysts after the longevity test; and (c) TEM image and particle size distribution of the fresh 2.5 % Ru/MgAl-R300 catalysts.

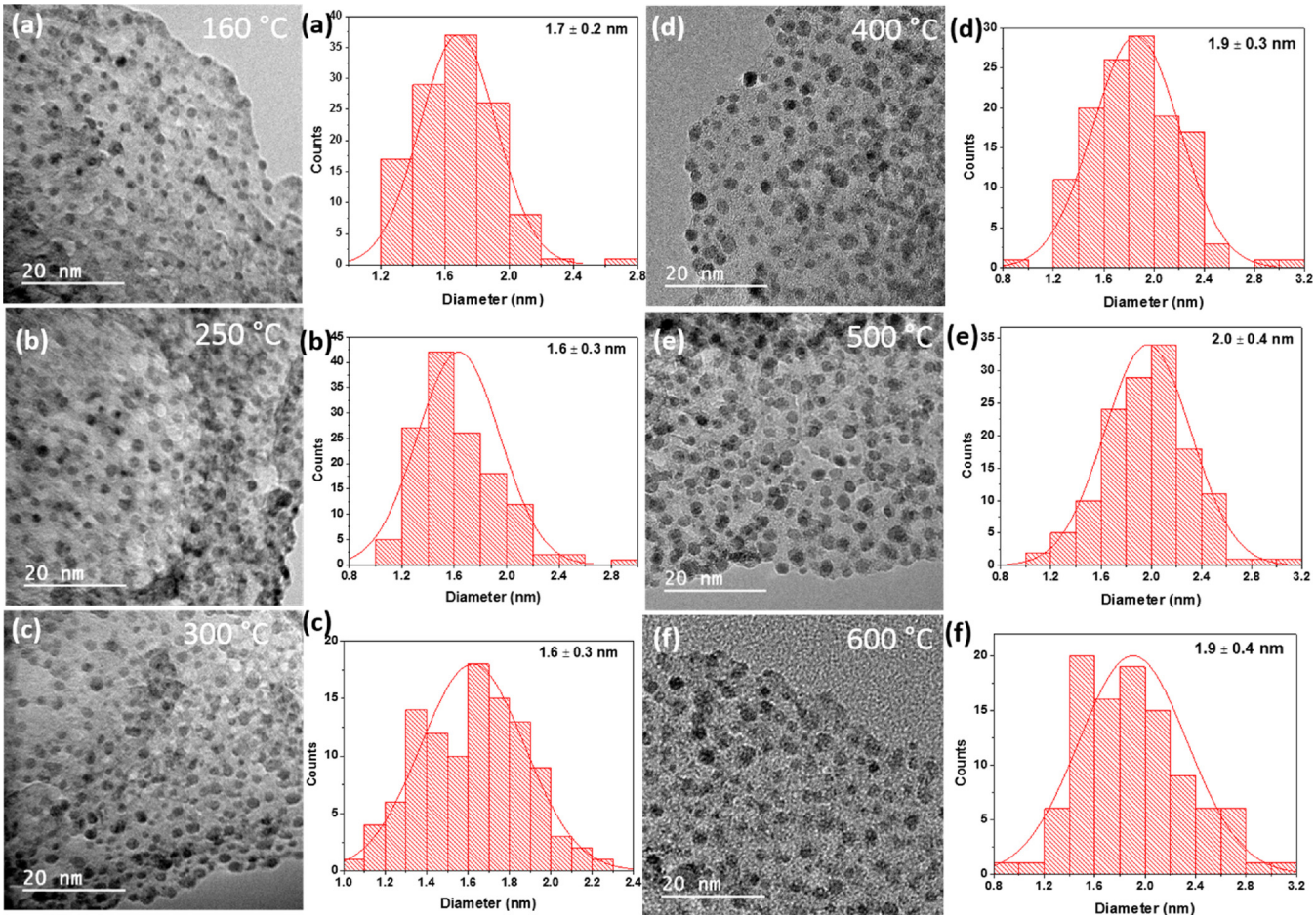

Fig. 5. TEM images and the corresponding particle size distribution of 2.5 % Ru/MgAl catalysts reduced at different reduction temperatures of (a) 160 °C, (b) 250 °C, (c) 300 °C, (d) 400 °C, (e) 500 °C, and (f) 600 °C. Histograms are made by counting more than 100 particles for multiple HRTEM images taken in different sample regions.

reduced the energy barrier for CO_2 hydrogenation [26]. Conversely, based on the calculated TOFs of the catalysts under study (Fig. 1d), the Ru/MgAl-R250 catalyst shows the highest TOFs, and the catalysts reduced at > 400 °C presents significantly low TOFs. Accordingly, the particle size of Ru catalysts might not play a key role in the NTP-catalysis.

As the electronic state of the active phase is an important factor to influence the catalytic behaviour, FTIR of CO adsorption and XPS were performed to understand the effect of reduction temperature on the electronic states of surface Ru species on the support. As shown in Fig. 6, the bands at 2173 cm^{-1} is assigned to physisorbed CO and the bands at 1950–2070 cm^{-1} are attributed to linearly bonded CO [27]. The IR bands located at 2051 cm^{-1} and 2120–2130 cm^{-1} were assigned to the CO species linearly adsorbed on the Ru° surfaces and Ru with a higher oxidation state [28], respectively, while the bands at 1983 cm^{-1} were associated with CO adsorbed on the very small Ru NPs [29]. In the case of Ru/MgAl-R600 catalyst, the peak at 1983 cm^{-1} disappeared, and a new shoulder peak at 2070 cm^{-1} emerged, corresponding to the multiply bonded carbonyl species (Ru°-$(CO)_n$ species) [30]. Additionally, the linear CO bands shifted to higher wavenumber with an increase in reduction temperature, which is due to the variation in particle size and the phase transformation, in agreement with the findings from XRD and TEM [31]. From XPS (Fig. S12 and Table S5), the surface Ru NPs show oxidation which may be due to air exposition at RT during sample preparation. The Ru3d peaks were deconvoluted into Ru^{4+} (RuO_2), Ru^{6+} (RuO_3) and Ru°. It can be seen that the binding energy of RuO_2 was much higher on the Ru/MgAl catalysts reduced

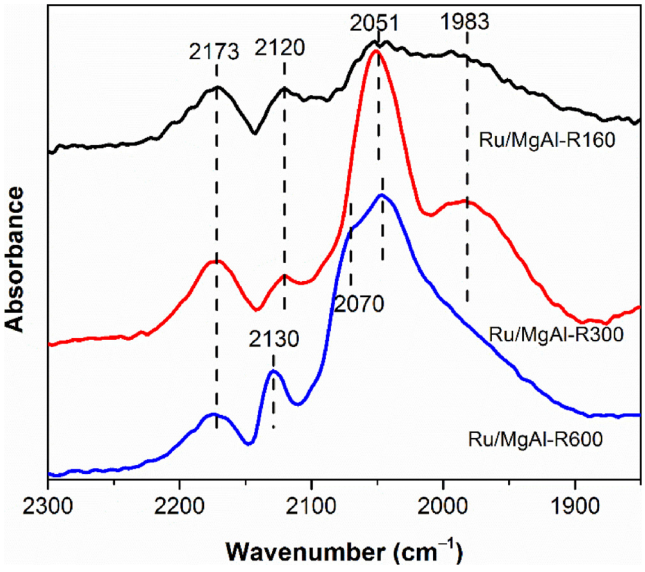

Fig. 6. FTIR spectra of adsorbed CO (CO-DRIFT) on the reduced 2.5 % Ru/MgAl-R160, 2.5 % Ru/MgAl-R300 and 2.5 % Ru/MgAl-R600 catalysts.

at < 300 °C (281.3 eV), which may be due to the relatively strong interaction between Ru NPs and supports or the inadequate reduction [32,33]. By increasing the reduction temperature from 160 °C to 600 °C, Ru^{6+}/Ru^{Total} ratio of the resulting catalyst decreased by ~28 % (Table

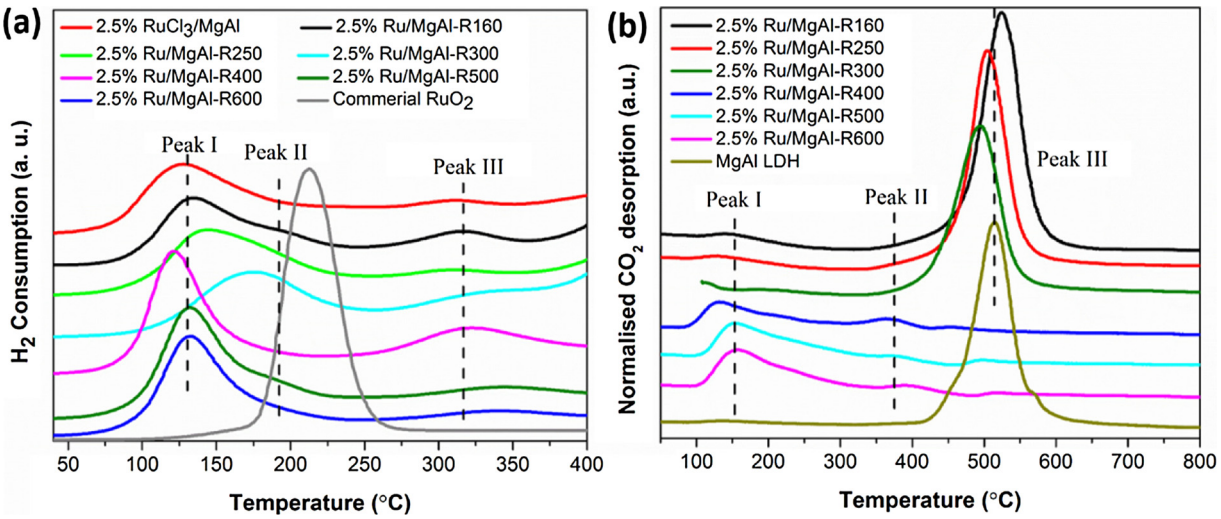

Fig. 7. (a) H_2-TPR and (b) CO_2-TPD profiles of 2.5 % Ru/MgAl catalysts reduced at different temperatures.

S5), and an additional Ru° peak appeared in the Ru/MgAl-R600 catalyst, confirming the improved reduction level of Ru species in the catalyst after the reduction treatment at high temperatures. Also, the analysis of O1s core level shows that the peak of interlayer H_2O between LDH layers gradually disappeared due to dehydration at elevated temperatures, being in line with the XRD results. The findings from the CO-FTIR and XPS revealed that the electronic features of Ru NPs were different with different reduction temperatures, and thus affecting the catalytic performance for CO_2 hydrogenation.

The metal-support interaction is another factor affecting the catalytic performance, which was determined by H_2-TPR (Fig. 7a). For the control experiment using the commercial RuO_2 catalyst, only one reduction peak at 213 °C was measured, corresponding to the reduction of Ru^{4+} to Ru°. Regarding the 2.5 % Ru/MgAl catalysts, TPR results show that, in general, the metal-support interaction becomes stronger with an increase in the reduction temperature. In the case of the as-prepared $RuCl_3$/MgAl LDH, the peak at 126 °C can be assigned to reduction of $RuCl_3$ adsorbed on the surface of MgAl LDH [34]. For the reduced 2.5 % Ru/MgAl catalysts, three reduction peaks centred at 120 − 180 °C (peak I), 185 − 220 °C (peak II), and 320 − 340 °C (peak III), which are attributed to the weakly supported RuO_x species on the support, strongly supported RuO_x species and the surface or subsurface oxygens, respectively [32,33]. For 2.5 % Ru/MgAl catalysts reduced at 160 − 300 °C, the peak I gradually shifts to higher values from 135 °C to 175 °C, suggesting that the improved metal-support interaction promoted by increasing the reduction temperature (< 300 °C). Interestingly, when the Ru/MgAl catalysts were reduced at high temperatures, namely > 400 °C, the peak I shifted back to 120 °C with a shoulder peak appeared at 132 °C, suggesting the reduced metal-LDO support interaction compared with that of metal-LDH. Coupled with the catalytic performances shown in Fig. 1, it was found that the strong interaction between Ru species and support favours the catalysis. Accordingly, we proposed that the metal-support interaction plays a key role for the NTP-catalysis activity over the catalysts reduced at 160 − 300 °C compared with the variation in the Ru particle sizes.

The surface basicity of Ru/MgAl catalysts, which is beneficial to the adsorption and activation of CO_2, was evaluated by CO_2-TPD, as shown in Fig. 7b. For 2.5 % Ru/MgAl catalysts reduced at 160 − 300 °C, only one strong peak appears at about 500 °C, which is from the LDH support (*i.e.* completely decomposition of CO_3^{2-} group in the internal layer). No other CO_2 desorption peaks were detected, as the strong interaction between Ru and LDH lead to very weak adsorption of CO_2, which can be easily removed by Ar purge. However, for 2.5 % Ru/MgAl catalysts reduced at > 400 °C, two dominant peaks located at 129 − 154 °C and 367 − 399 °C was observed, which can be ascribed to the surface sites of weak (OH) −and strong (unsaturated oxygen pairs) basicity sites, respectively [24,25]. The peak for CO_2 desorption at 129 − 154 °C originates from the decomposition of carbonate-like species formed by CO_2 with surface OH− group [32], while the peak at 367 − 399 °C can be attributed to the migration of Al^{3+} into the MgO framework, forming the unsaturated oxygen on the surface [35], which is in agreement with the XRD results. The findings from the CO_2-TPD shows a relatively strong CO_2 adsorption on the catalysts reduced at > 400 °C. Interestingly, these catalysts showed relatively poor activity (Fig. 1) in the NTP-catalysis. Therefore, these findings suggest that the strongly adsorbed CO_2 on the surface may block the active sites for surface reactions, which is in line with previous findings [36].

3.3. Mechanistic study for NTP-assisted CO_2 hydrogenation

Comparative *in situ* optical emission spectroscopy (OES) of gas phase NTP from the blank reactor without a catalyst and the NTP-catalysis (with 2.5 % Ru/MgAl-R300 and 2.5 % Ru/MgAl-R600 catalysts) systems were performed to understand the nature of the excited species formed under NTP conditions. Fig. 8 shows that (*i*) the emission from plasma was mainly in a range of 180–450 nm and (*ii*) the characteristic

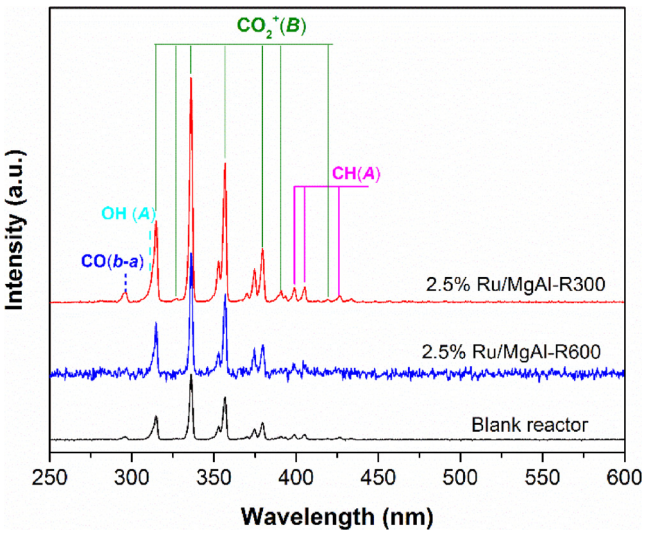

Fig. 8. *In situ* optical emission spectra of NTP-assisted CO_2 hydrogenation in NTP-alone and NTP-catalysis systems. (6.5 kV, 20.5 kHz).

electronically excited states of CO ($b^3\Sigma^+ \rightarrow a^3\Pi$), CO_2^+ (B: $A^2\Sigma^+ \rightarrow X^2\Pi$), OH ($A^2\Sigma^+ \rightarrow X^2\Pi$) and CH ($A^2\Delta \rightarrow X^2\Pi$) [37] were observed in all NTP systems. Compared with the emission in the NTP-alone system, the intensity of CO, CH and CO_2^+ emission was much higher in the NTP-catalysis systems, especially with the 2.5 % Ru/MgAl-R300 catalyst, corresponding to the improved concentration of active species in the excited states, and thus the enhanced CO_2 conversion as shown in Fig. 1. Based on the single ionised emission lines and the Boltzmann plot method [38], the electron temperature of the NTP system is determined at around 2.8 eV, being able to activate the stable gas molecules energy-efficiently *via* the electron-induced CO_2 dissociation and hydrogenation reactions on the surface of catalysts [39]. Conversely, hydrogenation of CO_2 by heating at atmospheric pressure requires a temperature in excess of 250 °C.

To elucidate the reaction pathway of catalytic CO_2 hydrogenation under NTP activation, *in situ* DRIFTS coupled with mass spectrometry (MS) characterisation of the Ru/MgAl-R300 and Ru/MgAl-R600 catalysts was performed comparatively under both thermal (at 270 °C) and NTP conditions with different feed gases. The 2.5 % Ru/MgAl-R300 and Ru/MgAl-R600 catalysts were selected since they showed the distinct catalytic activity due to the catalyst reduction temperature. Under the thermal conditions, the DRIFTS (Fig. S13) of the 2.5 % Ru/MgAl-R300 catalyst shows the typical CO pathway with only CO and CH_4 peaks detected on the catalyst surface, while formate species was also detected on the Ru/MgAl-R600 catalyst in addition to the surface CO and methane species. However, DRIFTS of the Ru/MgAl-R600 catalyst (Fig. S14) shows insignificant change of the formate species during the reaction, suggesting that they might not participate in CH_4 formation process. Under the NTP conditions, more carbon species were detected by DRIFTS, indicating that a more complex pathway for CO_2 conversion is present for the NTP-catalysis. According to the previous studies [40,41], in the plasma-activated CO_2 hydrogenation with catalysts, both gas-phase reactions and plasma-assisted surface reactions contribute to CO_2 conversion and selectivity to CH_4, *i.e.* (*i*) the dissociation of CO_2 and H_2 in the gas phase (Eqs. S1 − 2 in Table S8), followed by surface hydrogenation reactions to produce CH_4 (the dissociated H species in the gas phase may participate in the surface hydrogenation reactions); (*ii*) absorption of CO_2 molecules (in both ground and excited states) on Ru surfaces to form $CO_{2,ad}$, dissociation of $CO_{2,ad}$ into CO^*_{ad} and O^*_{ad} (Eqs. S3 − 4 in Table S8), and then NTP-assisted surface hydrogenation reactions to produce CH_4 (due to the low bulk temperatures at ~120 °C, the thermal-assisted surface hydrogenation reactions was assumed not possible).

The gas-phase CO_2 dissociation to CO was confirmed by DRIFTS and MS using 1% CO_2/Ar mixture under the NTP conditions (with 2.5 % Ru/MgAl-R300 catalyst, Fig. S15). Under the plasma-off condition, surface species were not detect with CO_2 flow. When the plasma was on, the linearly adsorbed CO_{ad} peak (at 2125, 2064, 2018 and 1847 cm^{-1}), bidentate carbonate (1561 and 1282 cm^{-1}) species were formed immediately, suggesting the adsorption of vibrationally excited CO_2 species on the catalyst surface. By switching off the plasma again, the relevant peaks of the carbon species remained, proving the strong adsorption of the species on the surface (Fig. S15c).

With the reaction gas mixture (*i.e.* 1% CO_2/4% H_2/Ar), prior to the ignition of plasma, only the gas phase peaks related to CO_2 (at 2361 and 2343 cm^{-1}, as shown in Fig. 9a) were detected, and MS profile (Fig. S16) confirmed that the catalyst (2.5 % Ru/MgAl-R300) was not active for CO_2 hydrogenation without NTP. Upon the ignition of plasma, the instantaneous appearance of CH_4 signal (m/z = 15) associated with a decrease of CO_2 signal (m/z = 44) in MS profiles (Fig. S16) confirmed the activity of the NTP-catalysis system. Additionally, characteristic peaks of carbonyl (CO_{ad}, at 2023 and 1945 cm^{-1}), carbon-hydroxyl (COH_{ad}, at 1300 cm^{-1}) and formyl species (HCO_{ad}, at 1756 and 1132 cm^{-1}) were detected by DRIFTS simultaneously on the catalyst surface (Fig. 9b) [42]. The IR peak at ~1037 cm^{-1} corresponds to methoxy species (OCH_3), showing no changes during the reaction, suggesting the formation of methanol, which was confirmed by the in-line MS analysis with increased intensity of m/z = 31 (corresponding to methanol), as shown in Fig. S17. The band at 3016 cm^{-1} is normally attributed to surface methane which was not detected under the condition used. This may be caused by the fast desorption of CH_4 from the catalyst surface under the NTP conditions [43]. When the plasma was switched off, MS profile showed that the system was not active anymore (Fig. S16). Interestingly, by comparing DRIFTS spectra of the NTP system with CO_2/Ar (Fig. S15c) and the CO_2/H_2/Ar (Fig. 9c) feed gases, the presence of H_2 affects the CO binding on Ru, which is evidenced by the CO_{ad} peak shift from 2064 and 2018 cm^{-1} to 2023 and 1945 cm^{-1}, suggesting the transformation of multicarbonyl to monocarbonyl species [30]. Moreover, the interaction between Ru and CO_{ad} was weakened (Fig. 9c) in the presence of H_2, causing the gradual disappearance of CO_{ad} bands after plasma extinction. This is due to the co-absorption of H* and CO*/O* on the Ru surface [44].

To illustrate the quantitative agreement between the intensity change of the surface species and the formation of CH_4 in the NTP-catalysis system, we include the evolution of the surface species as a function of time from *in situ* DRIFTS (Fig. 9b), together with the intensity increase of the CH_4 from MS (Fig. S16). The intensity of surface CO_2 species shows a significant decrease, while CH_4 signal from MS increased continuously over the course of the reaction, suggesting that CO_2 was hydrogenated to produce CH_4. In addition, the CO signal shows a steeper increase than that of CH_4, confirming the possible CO production both plasma-assisted CO_2 dissociation in the gas phase and the dissociation of adsorbed CO_2 on the catalyst. And the progressive increase of HCO_{ad} species and COH_{ad} profiles are consistent with the rate of CH_4 formation, suggesting that CO_2 hydrogenation in the system under study was *via* the HCO and COH pathway [45–47]. Also the concentration of HCO_{ad} is higher than that of COH_{ad} groups, due to the low HCO_{ad} formation energy (~1.25 eV) compared to that of COH_{ad} (~1.42 eV) [48]. Accordingly, the key elementary surface reaction steps are proposed for the NTP-catalysis over the 2.5 % Ru/MgAl-R300 catalyst, in which CO_2 is dissociated to carbonyl (CO_{ad}) and O* species, then was hydrogenated to formyl intermediate (HCO_{ad} and COH_{ad}) species. Coupled with the excited OH and CH species measured by OES in the gas phase, the overall reaction schemes are shown in Fig. 10 and Table S8.

For the NTP system employing the Ru/MgAl-R600 catalyst, *in situ* DRIFTS analysis revealed multiple surface species, suggesting a more complex reaction mechanism of CO_2 hydrogenation than the system with the Ru/MgAl-R300 catalyst. Under the plasma-off condition with CO_2/Ar gas at RT, surface bicarbonate with the characteristic IR bands at 1674, 1420 and 1224 cm^{-1} and carbonate at 1538 cm^{-1} were observed, as shown in Fig. S18, due to the CO_2 interaction with the surface hydroxyl group on the catalyst [49]. Upon the plasma ignition, more surface carbon species were produced, including the bridged and linearly adsorbed CO_{ad} peaks (at 2129, 2078, 2027 and 1867 cm^{-1}), bicarbonate (at 1660 and 1415 cm^{-1}) and bidentate carbonate (at 1538 and 1295 cm^{-1}). CO and O_2 due to the dissociation of CO_2 in the gas phase were also detected by MS as well (Fig. S18d).

With the reactant feed gas (*i.e.* 1% CO_2/4% H_2/Ar) (Fig. 11), carbonyl (CO_{ad}, at 2038 and 1945 cm^{-1}) and oxygenated species of CH_xO (at 1130 and 1304 cm^{-1}) were measured instantaneously under the plasma-on condition and then disappeared gradually (within 5 min) when plasma was off. This suggests that CHO species and CO_{ad} is active for reactions towards CH_4 formation, and CH_xO species originated from the reaction between CO* and H*, *i.e.* CO* + H* → CHO*, and then CHO* + H* → OCH_3. Finally, OCH_3 reacted with H* to produce CH_4 and H_2O, which is similar to the findings from the Ru/MgAl-R300 catalyst. However, the formation of methanol on Ru/MgAl-R600 catalyst during the catalysis under NTP conditions was insignificant as no methoxy peak was measured by *in situ* DRIFTS. Conversely, the bicarbonate species (at 1678 and 1410 cm^{-1}) disappeared gradually during the reaction and new IR bands at 2865 and 1601 cm^{-1} emerged

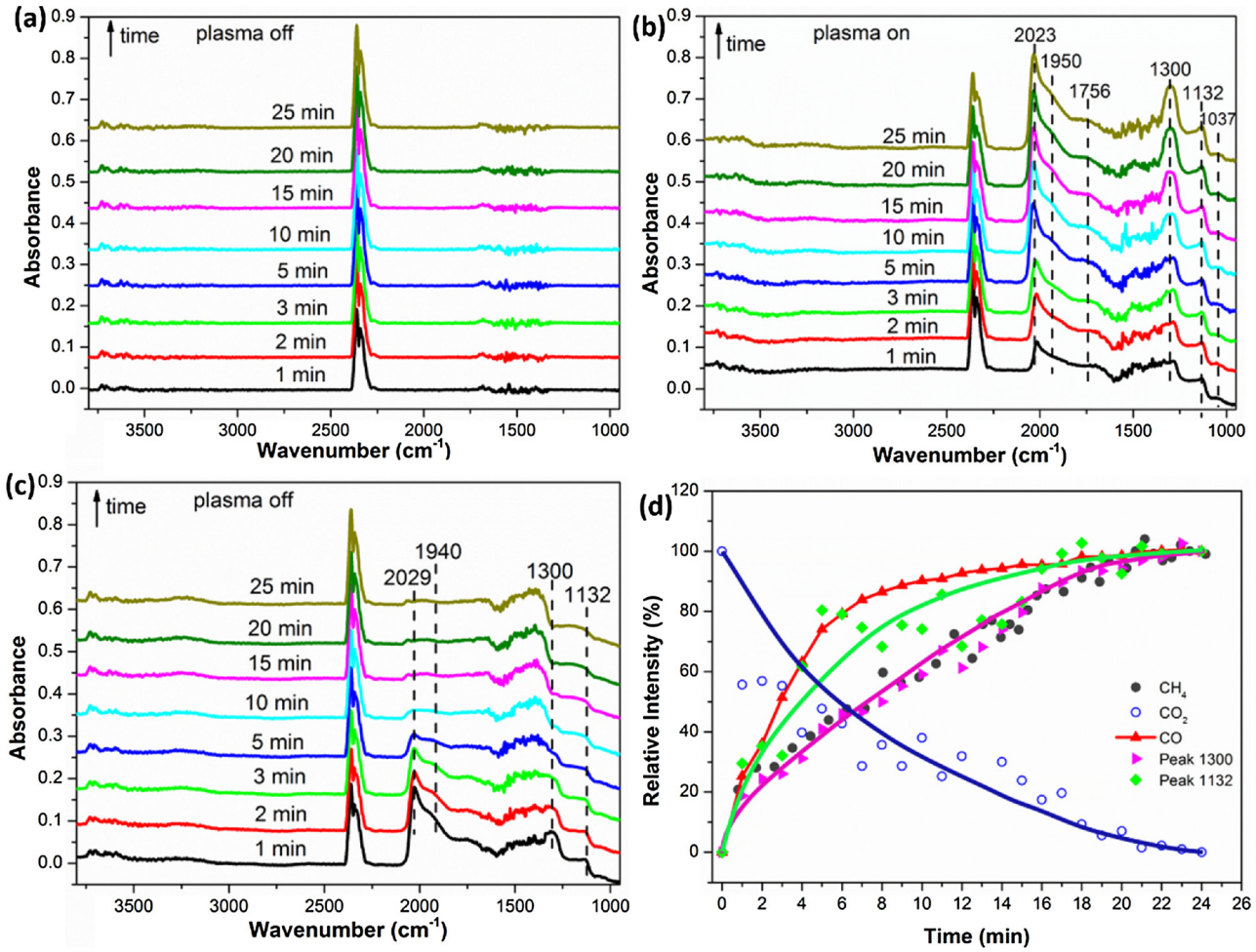

Fig. 9. *In situ* DRIFTS spectra of surface species on the 2.5 % Ru/MgAl-R300 catalyst under (a) plasma-off condition with the feed gas of 1% CO_2 + 4% H_2 + Ar; (b) plasma-on condition with the feed gas (5.0 kV, 23.5 kHz); and (c) plasma-off condition with the feed gas. (d) Relative intensities of surface species as a function of time-on-stream recorded in the *in-situ* DRIFTS from (b) and relative intensity change of methane recorded in mass spectra (Fig. S16) during CO_2 hydrogenation upon NTP on (5.0 kV, 23.5 kHz).

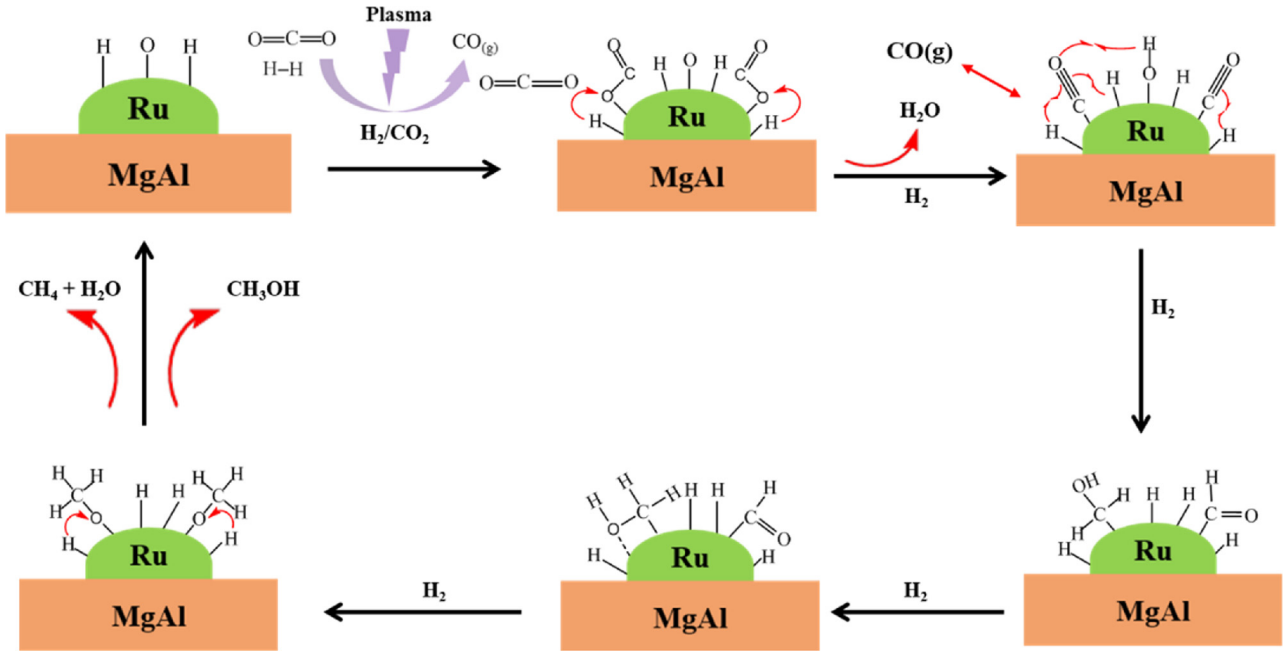

Fig. 10. Scheme of the reaction pathways of the NTP-activated CO_2 hydrogenation over 2.5 % Ru/MgAl-R300 catalyst.

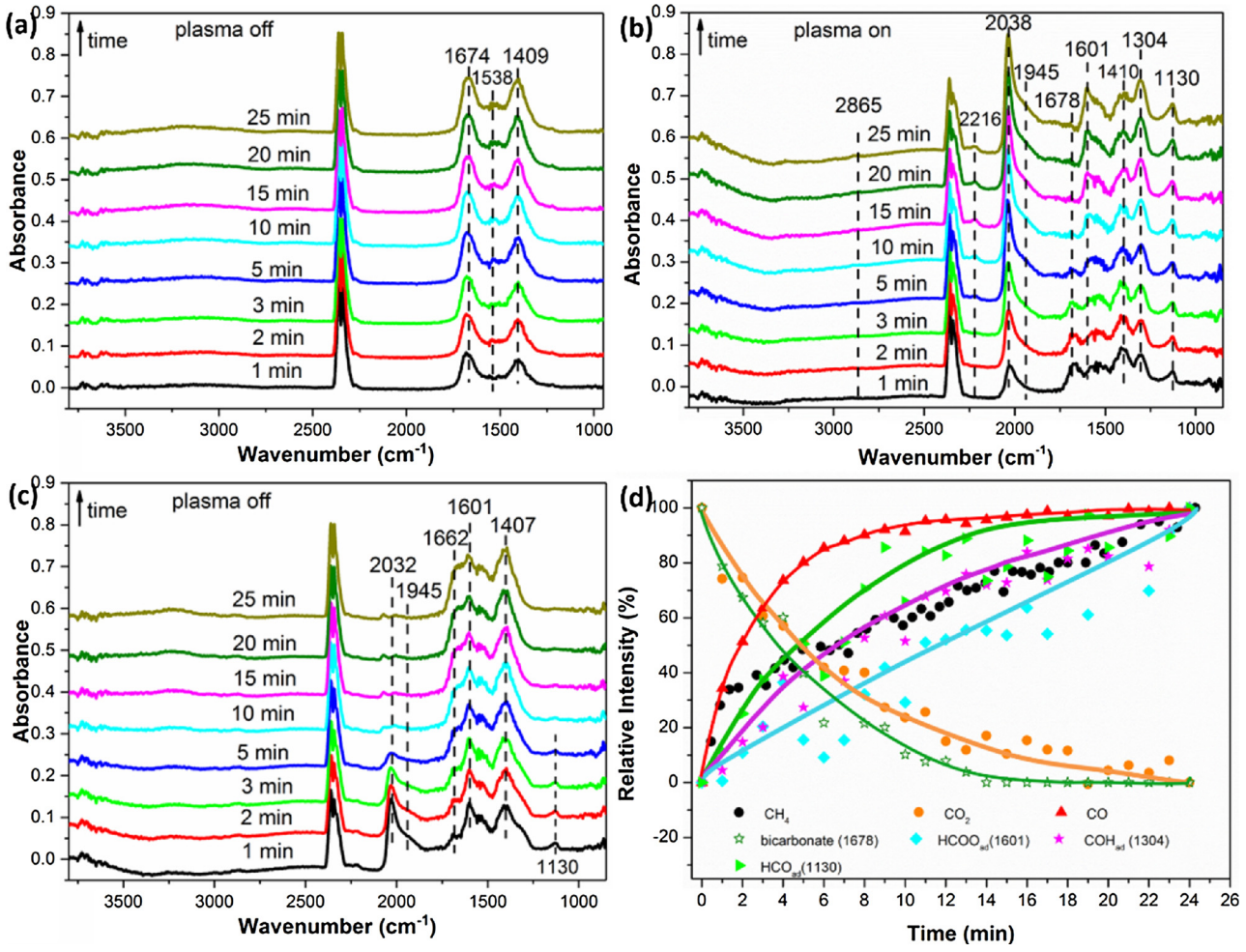

Fig. 11. *In situ* DRIFTS spectra of surface species on the 2.5 % Ru/MgAl-R600 catalyst under (a) plasma-off condition with the feed gas of 1% CO_2 + 4% H_2 + Ar; (b) plasma-on condition with the feed gas (5.0 kV, 23.5 kHz); and (c) plasma-off condition with the feed gas. (d) Relative intensities of surface species as a function of time-on-stream recorded in the *in-situ* DRIFTS from (b) and relative intensity change of methane recorded in mass spectra (Fig. S19) during CO_2 hydrogenation upon NTP on (5.0 kV, 23.5 kHz).

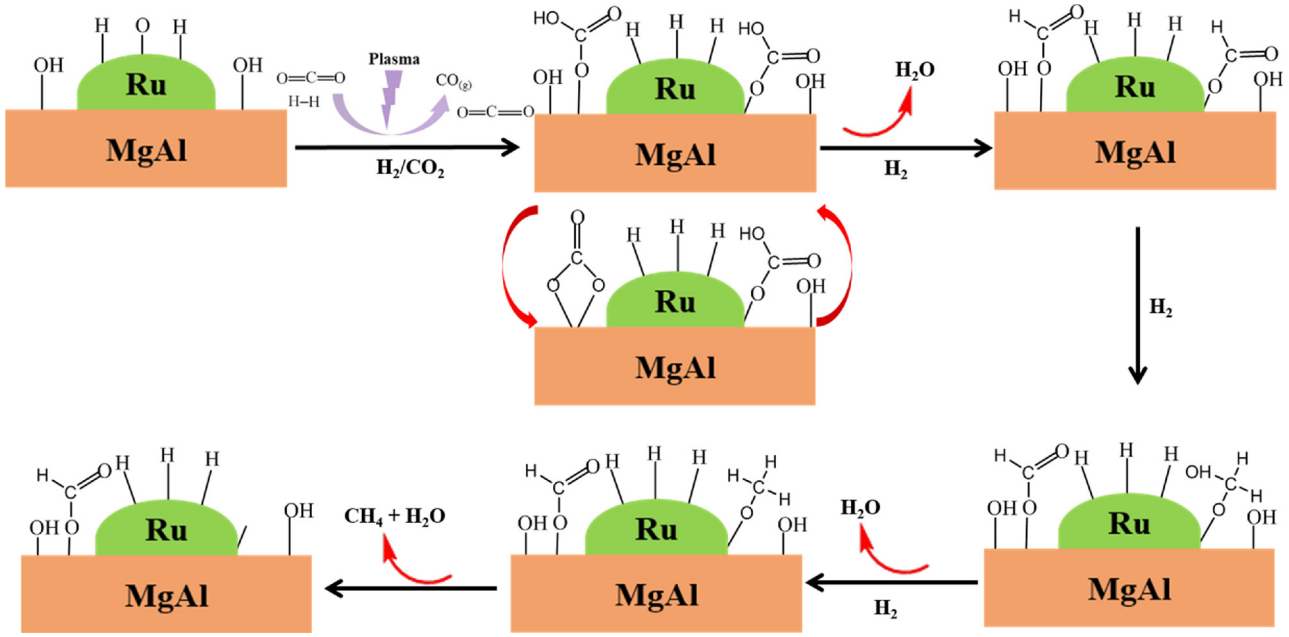

Fig. 12. Scheme of the bicarbonate-formate-methane reaction pathways of the NTP-activated CO_2 hydrogenation over 2.5 % Ru/MgAl-R600 catalyst.

which are associated with the adsorbed monodentate formates (HCOO*) [47], suggesting the bicarbonate species were transformed to formate under plasma. By switching off the plasma, the bicarbonate IR bands at 1662 and 1407 cm^{-1} built up again and overlapped with the formate bands, forming one broad band. Considering that the main location of bicarbonates is on the surface of the support, the decrease of IR intensity of bicarbonate bands under plasma was very likely due to the reaction between bicarbonates and activated H* in the gas phase or at the interface of Ru/support to form formates. A previous study stated that the formate species formed at the interfacial sites are more reactive towards H* than the formates formed on/migrated to the support (to form CH_4), and the latter can accumulate on the surface [50], explaining the remaining formate species on the surface after the NTP-catalysis (when plasma was off). Therefore, based on the *in situ* DRIFT spectroscopic data, the significant evolution of the IR bands supports the assertion of possible reaction pathway of bicarbonate-formate-methane coupled with the HCO and COH pathways for NTP-assisted CO_2 hydrogenation over the Ru/MgAl-R600 catalyst. As shown in Fig. 12 and Table S9, the adsorbed CO_2 reacts with the surface hydroxyl to produce the bicarbonate and carbonate species. The bicarbonate species then combines with the adsorbed hydrogen to produce formate species which undergoes a multistep reaction with hydrogen to produce methane and water.

Based on the comparative *in situ* DRIFTS-MS characterisation of the catalysis over the 2.5 % Ru/MgAl-R300 and 2.5 % Ru/MgAl-R600 catalysts under thermal and NTP conditions, NTP-catalysis system enables the alternative surface pathways for promoting CO_2 hydrogenations, in line with the kinetic data shown in Fig. 2. And the reduction temperature (during the catalysts preparation) affects the metal-support interaction and surface basicity, leading to the different adsorption behaviours of CO_2 on the surface. Therefore, 2.5 % Ru/MgAl-R300 and 2.5 % Ru/MgAl-R600 catalysts present different active sites for CO_2 hydrogenations, which may alter the reaction pathways [46]. Accordingly, under NTP conditions, different intermediates were formed during CO_2 hydrogenation over 2.5 % Ru/MgAl-R300 and 2.5 % Ru/MgAl-R600, suggesting different reaction pathways for CO_2 conversion.

4. Conclusions

In this study, the hybrid NTP-catalyst system for CO_2 hydrogenation has been investigated in a dielectric-barrier-discharge (DBD) reactor combined with Ru supported on the MgAl LDH catalysts, in which 85 % CO_2 conversion and 84 % CH_4 yield can be achieved at 6.5 kV. It was clearly demonstrated that catalytic CO_2 hydrogenation is promoted significantly under the NTP conditions, improving CO_2 conversion, which is more than 6 times higher than that under the thermal condition at 250 °C. Kinetic studies further confirmed that the NTP-catalysis system presents lower activation barrier (21 kJ mol^{-1}) than the thermal system (82 kJ mol^{-1}).

The reduction temperature significantly affects the chemical and physical properties of the prepared catalysts significantly, which in turn strongly influences the CO_2 conversion and surface reactions under the plasma conditions. Comparative *in situ* DRIFTS-MS study confirmed that, under the thermal condition, CO_2 hydrogenation over the Ru/MgAl catalysts proceeds *via* the CO* route with CO as the sole intermediate. In contrast, plasma activation promotes the formation of various active species both in gas-phase and in catalysts-surface including CO*, O*, H*, formates, carbonate, formyl, carbonyl and water, explaining the improved performance of the NTP-catalysis system. Findings of the study confirms that the plasma-induced gas-phase dissociation of CO_2 and the interaction between plasma and catalyst surface opens new reaction routes, contributing to the enhanced CO_2 hydrogenation at low temperatures. However, further investigation into the surface interaction between the plasma, plasma-activated hydrocarbon species and the catalyst surface is needed to fully understand the CO_2 hydrogenation mechanism under plasma condition.

Credit Author Statement

- SX performed all experiemntal work under the supervision of HC, XF amd CH.
- SC, CE and HC contributed to in situ DRIFTS-MS characterisaion of the catalysis, as well as data intepreation, under both thermal and NTP conditions under the supervision of XF and CH.
- YS and YM contributed to the temperature programmed analysis and measurement of metal dispersion under the supervision of HC, XF amd CH.
- SX performed the OES characterisaion and relevant data interpration under the supervision of XF.
- YW contributed to the TEM characterisaion under the supervision of SH.
- YJ performed the nitrogen adsorption analsis of all catalysts.

Declaration of Competing Interest

None.

Acknowledgements

SX thanks the financial supports from the Dean's Doctoral Scholar Awards from the University of Manchester. HC acknowledges the financial support from the European Commission Marie Skłodowska-Curie for his Individual Fellowship (H2020-MSCA-IF-NTPleasure-748196). The UK Catalysis Hub is kindly thanked for resources and support provided *via* our membership of the UK Catalysis Hub Consortium and funded by EPSRC grants EP/R026939/1, EP/R026815/1, EP/R026645/1, EP/R027129/1, EP/M013219/1.

Appendix A. Supplementary data

Supplementary material related to this article can be found, in the online version, at doi:https://doi.org/10.1016/j.apcatb.2020.118752.

References

[1] W.H. Li, H.Z. Wang, X. Jiang, J. Zhu, Z.M. Liu, X.W. Guo, C.S. Song, A short review of recent advances in CO_2 hydrogenation to hydrocarbons over heterogeneous catalysts, RSC Adv. 8 (2018) 7651–7669.
[2] M. Gotz, J. Lefebvre, F. Mors, A.M. Koch, F. Graf, S. Bajohr, R. Reimert, T. Kolb, Renewable power-to-gas: a technological and economic review, Renew. Energy 85 (2016) 1371–1390.
[3] J. Bao, G.H. Yang, Y. Yoneyama, N. Tsubaki, Significant advances in C1 catalysis: highly efficient catalysts and catalytic reactions, ACS Catal. 9 (2019) 3026–3053.
[4] C. Mebrahtu, S. Abate, S. Perathoner, S.M. Chen, G. Centi, CO_2methanation over Ni catalysts based on ternary and quaternary mixed oxide: a comparison and analysis of the structure-activity relationships, Catal. Today 304 (2018) 181–189.
[5] M.A.A. Aziz, A.A. Jalil, S. Triwahyono, A. Ahmad, CO_2 methanation over heterogeneous catalysts: recent progress and future prospects, Green Chem. 17 (2015) 2647–2663.
[6] S. Rönsch, J. Schneider, S. Matthischke, M. Schlüter, M. Götz, J. Lefebvre, P. Prabhakaran, S. Bajohr, Review on methanation – from fundamentals to current projects, Fuel 166 (2016) 276–296.
[7] M. Xu, M. Wei, Layered double hydroxide-based catalysts: recent advances in preparation, structure, and applications, Adv. Funct. Mater. 28 (2018) 1802943–1802963.
[8] K. Mori, T. Taga, H. Yamashita, Isolated single-atomic Ru catalyst bound on a layered double hydroxide for hydrogenation of CO_2 to formic acid, ACS Catal. 7 (2017) 3147–3151.
[9] P. Li, F. Yu, N. Altaf, M. Zhu, J. Li, B. Dai, Q. Wang, Two-dimensional layered double hydroxides for reactions of methanation and methane reforming in C1 chemistry, Materials (Basel) 11 (2018) 221–248.
[10] S. Abate, K. Barbera, E. Giglio, F. Deorsola, S. Bensaid, S. Perathoner, R. Pirone, G. Centi, Synthesis, characterization, and activity pattern of Ni–Al hydrotalcite catalysts in CO_2 methanation, Ind. Eng. Chem. Res. 55 (2016) 8299–8308.
[11] R. Snoeckx, A. Bogaerts, Plasma technology - a novel solution for CO2 conversion? Chem. Soc. Rev. 46 (2017) 5805–5863.
[12] E.C. Neyts, K.K. Ostrikov, M.K. Sunkara, A. Bogaerts, Plasma catalysis: synergistic effects at the nanoscale, Chem. Rev. 115 (2015) 13408–13446.
[13] R. Vakili, R. Gholami, C.E. Stere, S. Chansai, H. Chen, S.M. Holmes, Y. Jiao, C. Hardacre, X. Fan, Plasma-assisted catalytic dry reforming of methane (DRM) over metal-organic frameworks (MOFs)-based catalysts, Appl. Catal. B: Environ. 260

(2020) 118195–118206.
[14] C.E. Stere, J.A. Anderson, S. Chansai, J.J. Delgado, A. Goguet, W.G. Graham, C. Hardacre, S.F.R. Taylor, X. Tu, Z. Wang, H. Yang, Non-thermal plasma activation of gold-based catalysts for low-temperature water-gas shift catalysis, Angew. Chem. Int. Ed. 56 (2017) 5579–5583.
[15] S. Xu, S. Chansai, C. Stere, B. Inceesungvorn, A. Goguet, K. Wangkawong, S.F.R. Taylor, N. Al-Janabi, C. Hardacre, P.A. Martin, X. Fan, Sustaining metal–organic frameworks for water–gas shift catalysis by non-thermal plasma, Nat. Catal. 2 (2019) 142–148.
[16] Y. Zeng, X. Tu, Plasma-catalytic hydrogenation of CO_2 for the cogeneration of CO and CH_4 in a dielectric barrier discharge reactor: effect of argon addition, J. Phys. D Appl. Phys. 50 (2017) 184004–184014.
[17] H.H. Chen, Y.B. Mu, Y. Shao, S. Chansai, S.J. Xu, C.E. Stere, H. Xiang, R.X. Zhang, Y.L. Jiao, C. Hardacre, X.L. Fan, Coupling non-thermal plasma with Ni catalysts supported on BETA zeolite for catalytic CO_2 methanation, Catal. Sci. Technol. 9 (2019) 4135–4145.
[18] C.E. Stere, W. Adress, R. Burch, S. Chansai, A. Goguet, W.G. Graham, C. Hardacre, Probing a non-thermal plasma activated heterogeneously catalyzed reaction using in situ DRIFTS-MS, ACS Catal. 5 (2015) 956–964.
[19] E.K. Gibson, C.E. Stere, B. Curran-McAteer, W. Jones, G. Cibin, D. Gianolio, A. Goguet, P.P. Wells, C.R.A. Catlow, P. Collier, P. Hinde, C. Hardacre, Probing the role of a non-thermal plasma (NTP) in the hybrid NTP catalytic oxidation of methane, Angew. Chem. Int. Ed. 56 (2017) 9351–9355.
[20] B. Ashford, X. Tu, Non-thermal plasma technology for the conversion of CO_2, Curr. Opin. Green Sustain. Chem. 3 (2017) 45–49.
[21] X. Zhu, X. Liu, H.-Y. Lian, J.-L. Liu, X.-S. Li, Plasma catalytic steam methane reforming for distributed hydrogen production, Catal. Today 337 (2019) 69–75.
[22] J. Kim, D.B. Go, J.C. Hicks, Synergistic effects of plasma-catalyst interactions for CH_4 activation, Phys. Chem. Chem. Phys. 19 (2017) 13010–13021.
[23] F. Cavani, F. Trifiro, A. Vaccari, Hydrotalcite-type anionic clays: preparation, properties and applications, Catal. Today 11 (1991) 173–301.
[24] M. Zhang, Y. Zhao, Q. Liu, L. Yang, G. Fan, F. Li, A La-doped Mg-Al mixed metal oxide supported copper catalyst with enhanced catalytic performance in transfer dehydrogenation of 1-decanol, Dalton Trans. 45 (2016) 1093–1102.
[25] P. Liu, M. Derchi, E.J.M. Hensen, Synthesis of glycerol carbonate by transesterification of glycerol with dimethyl carbonate over MgAl mixed oxide catalysts, Appl. Catal. A Gen. 467 (2013) 124–131.
[26] J.H. Kwak, L. Kovarik, J. Szanyi, CO_2 reduction on supported Ru/Al_2O_3 catalysts: cluster size dependence of product selectivity, ACS Catal. 3 (2013) 2449–2455.
[27] N. Tang, Y. Cong, Q. Shang, C. Wu, G. Xu, X. Wang, Coordinatively unsaturated Al^{3+} sites anchored subnanometric ruthenium catalyst for hydrogenation of aromatics, ACS Catal. 7 (2017) 5987–5991.
[28] L. Chen, Y. Zhu, H. Zheng, C. Zhang, Y. Li, Aqueous-phase hydrodeoxygenation of propanoic acid over the Ru/ZrO_2 and $Ru–Mo/ZrO_2$ catalysts, Appl. Catal. A Gen. 411–412 (2012) 95–104.
[29] A.M. Abdel-Mageed, D. Widmann, S.E. Olesen, I. Chorkendorff, R.J. Behm, Selective CO methanation on highly active Ru/TiO_2 catalysts: identifying the physical origin of the observed Activation/Deactivation and loss in selectivity, ACS Catal. 8 (2018) 5399–5414.
[30] N. Gupta, V. Kamble, R. Iyer, K.R. Thampi, M. Gratzel, The transient species formed over $Ru–RuOx/TiO_2$ catalyst in the CO and $CO + H_2$ interaction: FTIR spectroscopic study, J. Catal. 137 (1992) 473–486.
[31] J. Singh, J.A. van Bokhoven, Structure of alumina supported platinum catalysts of different particle size during CO oxidation using in situ IR and HERFD XAS, Catal. Today 155 (2010) 199–205.
[32] D. Li, R. Li, M. Lu, X. Lin, Y. Zhan, L. Jiang, Carbon dioxide reforming of methane over Ru catalysts supported on Mg-Al oxides: a highly dispersed and stable Ru/Mg(Al)O catalyst, Appl. Catal. B: Environ. 200 (2017) 566–577.
[33] Y. Guo, S. Mei, K. Yuan, D.-J. Wang, H.-C. Liu, C.-H. Yan, Y.-W. Zhang, Low-temperature CO_2 methanation over CeO_2-supported Ru single atoms, nanoclusters, and nanoparticles competitively tuned by strong metal–support interactions and H-spillover effect, ACS Catal. 8 (2018) 6203–6215.
[34] P. da Costa Zonetti, R. Landers, A.J.G. Cobo, Thermal treatment effects on the Ru/CeO_2 catalysts performance for partial hydrogenation of benzene, Appl. Surf. Sci. 254 (2008) 6849–6853.
[35] M. Abdellattif, M. Mokhtar, MgAl-layered double hydroxide solid base catalysts for Henry reaction: a green protocol, Catalysts 8 (2018) 133.
[36] Q. Pan, J. Peng, T. Sun, S. Wang, S. Wang, Insight into the reaction route of CO_2 methanation: promotion effect of medium basic sites, Catal. Commun. 45 (2014) 74–78.
[37] M.A. Johnson, R.N. Zare, J. Rostas, S. Leach, Resolution of the$\tilde{A}/\tilde{B}$ photoionization branching ratio paradox for the$12CO + 2\tilde{B}(000)$ state, J. Chem. Phys. 80 (1984) 2407–2428.
[38] J. Zalach, S. Franke, Iterative Boltzmann plot method for temperature and pressure determination in a xenon high pressure discharge lamp, J. Appl. Phys. 113 (2013) 043303–043311.
[39] S. Xu, J.C. Whitehead, P.A. Martin, CO_2conversion in a non-thermal, barium titanate packed bed plasma reactor: the effect of dilution by Ar and N_2, Chem. Eng. J. 327 (2017) 764–773.
[40] F. Azzolina-Jury, F. Thibault-Starzyk, Mechanism of low pressure plasma-assisted CO_2 hydrogenation over Ni-USY by microsecond time-resolved FTIR spectroscopy, Top. Catal. 60 (2017) 1709–1721.
[41] A. Parastaev, W.F.L.M. Hoeben, B.E.J.M. van Heesch, N. Kosinov, E.J.M. Hensen, Temperature-programmed plasma surface reaction: an approach to determine plasma-catalytic performance, Appl. Catal. B: Environ. 239 (2018) 168–177.
[42] S. Navarro-Jaén, J.C. Navarro, L.F. Bobadilla, M.A. Centeno, O.H. Laguna, J.A. Odriozola, Size-tailored Ru nanoparticles deposited over γ-Al_2O_3 for the CO_2 methanation reaction, Appl. Surf. Sci. 483 (2019) 750–761.
[43] H.-H. Kim, Y. Teramoto, A. Ogata, H. Takagi, T. Nanba, Plasma catalysis for environmental treatment and energy applications, Plasma Chem. Plasma Process. 36 (2015) 45–72.
[44] N. Gupta, V. Kamble, V. Kartha, R. Iyer, K.R. Thampi, M. Gratzel, FTIR spectroscopic study of the interaction of CO_2 and $CO_2 + H_2$ over partially oxidized $RuTiO_2$ catalyst, J. Catal. 146 (1994) 173–184.
[45] S. Eckle, H.-G. Anfang, R.J. Behm, Reaction intermediates and side products in the methanation of CO and CO_2 over supported Ru catalysts in H_2-rich reformate gases, J. Phys. Chem. C 115 (2010) 1361–1367.
[46] B. Miao, S.S.K. Ma, X. Wang, H. Su, S.H. Chan, Catalysis mechanisms of CO_2 and CO methanation, Catal. Sci. Technol. 6 (2016) 4048–4058.
[47] K. Zhao, L. Wang, M. Calizzi, E. Moioli, A. Züttel, In situ control of the adsorption species in CO_2 hydrogenation: determination of intermediates and byproducts, J. Phys. Chem. C 122 (2018) 20888–20893.
[48] J.L.C. Fajín, J.R.B. Gomes, M.N.D.S. Cordeiro, Mechanistic study of carbon monoxide methanation over pure and rhodium- or ruthenium-doped nickel catalysts, J. Phys. Chem. C 119 (2015) 16537–16551.
[49] J. Szanyi, J.H. Kwak, Dissecting the steps of CO_2 reduction: 1. The interaction of CO and CO_2 with gamma-Al_2O_3: an in situ FTIR study, Phys. Chem. Chem. Phys. 16 (2014) 15117–15125.
[50] A. Solis-Garcia, J.F. Louvier-Hernandez, A. Almendarez-Camarillo, J.C. Fierro-Gonzalez, Participation of surface bicarbonate, formate and methoxy species in the carbon dioxide methanation catalyzed by ZrO_2-supported Ni, Appl. Catal. B: Environ. 218 (2017) 611–620.